PERGAMON

International Journal of Impact Engineering 24 (2000) 259–275

INTERNATIONAL JOURNAL OF IMPACT ENGINEERING

www.elsevier.com/locate/ijimpeng

Impact of metallic projectiles on ceramic targets: transition between interface defeat and penetration

P. Lundberg*, R. Renström, B. Lundberg

FOA, Weapons and Protection Division, S-147 25 Tumba, Sweden

Received 4 June 1999; received in revised form 17 September 1999

Abstract

Armour systems capable of defeating an incoming projectile on the surface of a ceramic have been reported by several authors. This capability, called interface defeat, signifies that the projectile material is forced to flow radially outwards on the surface of the ceramic without penetrating significantly. In order to investigate the conditions for interface defeat, two models for the interaction of a metallic projectile and a ceramic target were established. With the aid of them, upper and lower bounds for the transition impact velocity between interface defeat and normal penetration were estimated for a given combination of metallic projectile and ceramic target. These approximate bounds were found to be consistent with transition velocities determined experimentally for two projectile materials (tungsten and molybdenum) and five target materials (two types of silicon carbide, boron carbide, titanium diboride and a polycrystalline diamond composite).

Keywords: Penetration; Interface defeat; Projectile; Target; Ceramic; Tungsten; Molybdenum; Silicon carbide; Boron carbide; Titanium diboride; Syndie

1. Introduction

Ceramics have two main qualities which make them interesting for armour applications, viz., low densities and high intrinsic strengths. These qualities offer possibilities to design weight-efficient armour systems with high protection capabilities. However, a major drawback of ceramics as target materials is their brittle behaviour, which is due to their inability to accommodate plastic

* Corresponding author. Tel.: 00-46-8-7063987; fax: 00-46-8-7064149.
E-mail address: patrik.lundberg@sto.foa.se (P. Lundberg)

0734-743X/00/$ - see front matter
PII: S0734-743X(99)00152-9

Nomenclature

a	projectile radius
K_p	bulk modulus of projectile material
p	normal surface load per unit area
p_0	maximum normal surface load per unit area
P	penetration
q_p	stagnation pressure
r	radial co-ordinate
R_t	target strength according to Tate
t	time
u	penetration velocity
v_p	impact velocity
Y_p	projectile strength according to Tate
z	axial co-ordinate
α	ratio between bulk modulus K_p and stagnation pressure q_p
β	ratio between yield strength σ_{yp} and stagnation pressure q_p
ν	Poisson's ratio
ρ_p	density of projectile material
σ_y	yield strength in compression of target material
σ_{yp}	yield strength of projectile material
τ_y	yield strength in shear of target material ($=\sigma_y/2$)
τ_{yp}	yield strength in shear of projectile material ($=\sigma_{yp}/\sqrt{3}$)
τ_0	maximum shear stress in target

strains. This brittleness facilitates nucleation, propagation and coalescence of micro-cracks and may lead to a heavily damaged and comminuted material as a result of impact and penetration [1].

In order to protect ceramic materials from damage, different devices for load distribution and attenuation, combined with confinement, have been tested [2–4]. In this way it has been possible to design ceramic armour systems capable of defeating ordnance velocity projectiles on the surface of the ceramic. This capability, called interface defeat [2–4], signifies that the projectile material is forced to flow radially outwards on the surface of the ceramic without penetrating significantly.

When the surface load generated by the projectile exceeds a critical value, at a critical impact velocity of the projectile, a transition between interface defeat and normal penetration behaviour occurs [5]. Below this transition velocity the ceramic behaves as extremely strong, and above it behaves as significantly weakened. It is likely that the transition is related to the maximum accessible strength of the ceramic material.

In this paper, the critical impact velocity for the transition between interface defeat and normal penetration is studied theoretically and experimentally. Two models are established which permit the determination of the surface load and the conditions for incipient and large-scale yield, respectively, in the target. From them, the transition impact velocity is estimated for a given

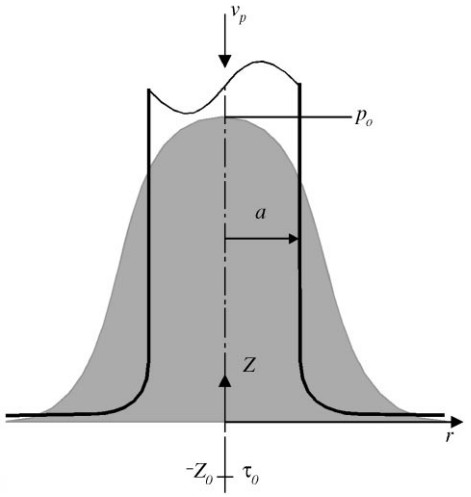

Fig. 1. Radial flow of a long projectile and resulting normal surface load per unit area on a flat, rigid and friction-free surface.

combination of metallic projectile and ceramic target. This transition impact velocity is compared with such velocities determined experimentally for different combinations of two projectile materials, viz., tungsten (WHA) and molybdenum (Mo), and five target materials, viz., two types of silicon carbide (SiC), boron carbide (B_4C) (reported earlier [5]), titanium diboride (TiB_2) and Syndie (a diamond composite).

2. Models

A long projectile with radius a is assumed to flow radially on a flat, rigid and friction-free surface as shown in Fig. 1. The flow is assumed to be steady so that the loading of the surface is quasi-static, which means that the initial transient part of the impact process is not considered. The material of the projectile is considered to be linearly elastic and perfectly plastic with bulk modulus K_p, yield strength σ_{yp} and density ρ_p.

With the assumption that the effects of yield strength and compressibility are small relative to that of inertia, and the use of several other simplifications, the approximate relation for the normal surface load per unit area on the axis of symmetry of the projectile

$$p_0 \approx q_p\left(1 + \frac{1}{2\alpha} + 3.27\beta\right) \tag{1}$$

with

$$\alpha = \frac{K_p}{q_p}, \quad \beta = \frac{\sigma_{yp}}{q_p} \tag{2}$$

Table 1
Normal load per unit area p as a function of radial distance r [6]

Radius r/a	Normal load p/p_0
0.000	1.0000
0.125	0.9994
0.250	0.9912
0.375	0.9741
0.500	0.9594
0.625	0.9341
0.750	0.8882
0.875	0.8353
1.000	0.7706
1.125	0.7029
1.250	0.6115
1.375	0.4976
1.500	0.3703
1.625	0.2353
1.750	0.1500
1.875	0.1000
2.000	0.0665
2.125	0.0471
2.250	0.0353
2.375	0.0253
2.500	0.0176
2.637	0.0106
2.864	0.0026
3.169	0.0000

and

$$q_{\mathrm{p}} = \frac{1}{2}\rho_{\mathrm{p}} v_{\mathrm{p}}^2 \tag{3}$$

is derived in the appendix. Here v_{p} is the impact velocity of the projectile and q_{p} is the stagnation pressure of an ideal fluid with density ρ_{p} and velocity v_{p}. The dimensionless parameters $\alpha \gg 1$ and $\beta \ll 1$ relate elastic and plastic effects, respectively, to the effect of inertia.

It is assumed that p_0 is the maximum normal surface load per unit area under the projectile and that the radial distribution of this load can be approximated by one determined experimentally for a low-velocity water jet [6]. Normalised results for this radial distribution of load per unit area $p(r)$ are shown in Table 1. The assumed load distribution, in combination with Boussinesq's elastic stress field solution for a point load on a semi-infinite elastic half-space [7], gives the relation $p_0 = (2.601 + 2.056\nu)\tau_0$ between the maximum load per unit area p_0 and the maximum shear stress τ_0 which appears at a distance $z_0 = (0.622 + 0.546\nu)a$ below the surface. These relations have been obtained from numerical calculations for different values of Poisson's ratio ν and are approximately valid for $0.05 \leqslant \nu \leqslant 0.20$. Here, an approximate lower bound p_0^{lower} for the transition from

interface defeat to normal penetration is obtained by putting the maximum shear stress τ_0 equal to the shear yield strength τ_y of the ceramic material, i.e,

$$p_0^{\text{lower}} = (2.601 + 2.056\nu)\tau_y. \tag{4}$$

For a ceramic material with the ability to accommodate plastic-like strains associated with comminution, the comminuted zone would start at the location z_0 of the maximum elastic shear stress and grow towards the loaded surface. When the comminuted zone reaches the surface, penetration would start.

A plastic slip-line solution for the indentation of a rigid punch [8–11] is used to obtain an approximate upper bound p_0^{upper} for the transition value of the maximum load per unit area. According to this solution there is the relation $p_0 = 5.70\tau_y$ between the average load per unit area p_0 and the shear yield strength τ_y when indentation occurs. Here, therefore, an approximate upper bound for the transition from interface defeat to normal penetration is taken to be

$$p_0^{\text{upper}} = 5.70\tau_y. \tag{5}$$

Finally, relations (4) and (5) give the approximate transition interval $p_0^{\text{lower}} \leqslant p_0 \leqslant p_0^{\text{upper}}$, i.e.,

$$(1.30 + 1.03\nu)\sigma_y \leqslant p_0 \leqslant 2.85\sigma_y \tag{6}$$

for the maximum normal load per unit area p_0, where $\sigma_y = 2\tau_y$ is the yield strength in uniaxial compression according to Tresca's hypothesis. As relations (1)–(3) provide a relation between normal load per unit area p_0 and the impact velocity v_p, these relations and the inequalities (6) give a transition interval also for the impact velocity v_p.

3. Experiments

Impact experiments were performed with a two-stage light-gas gun using the reverse impact technique [5,12–15]. Confined ceramic cylinders were launched against a stationary projectile mounted in front of the barrel. The projectile was suspended in a block of plastic foam (density 40 kg/m^3), see Figs. 2 and 3.

The stationary projectiles were cylinders with length 80 mm and diameter 2 mm (radius $a = 1$ mm). They were made of either sintered tungsten alloy (DX2 HCMF from Cime Bocuze) or molybdenum (Mo from Plansee). The ceramic cylinders, with nominal length 20 mm and diameter

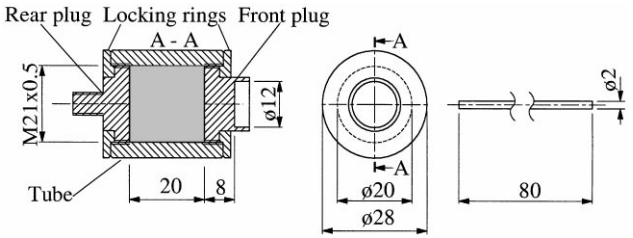

Fig. 2. Target and projectile used in reverse impact experiments.

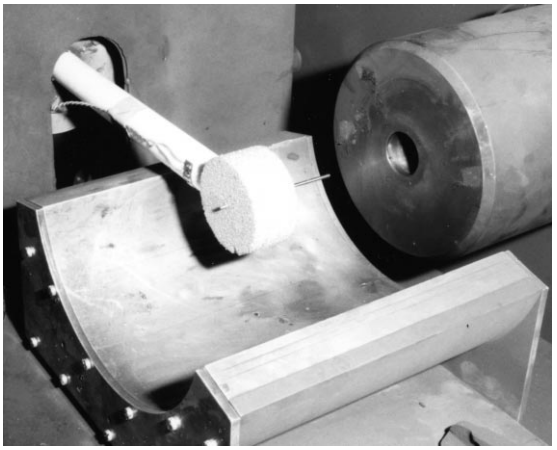

Fig. 3. Stationary projectile in plastic foam fixture mounted in front of light-gas gun muzzle.

Table 2
Projectile material data

Projectile material	Bulk modulus K_p (GPa)	Density ρ_p (kg/m^3)	Yield strength σ_{yp} (GPa)
WHA	285	17600	1.2
Mo	238	10220	0.9

20 mm, were made from two types of silicon carbide (SiC-1 and SiC-2), from titanium diboride (TiB_2), and from Syndie (from De Beers), which is a polycrystalline diamond composite (diamonds sintered together in the presence of cobalt as a solvent/catalyst metal). The SiC-1 material was produced by a pressure-assisted densification method, and the SiC-2 material was made by a hot isostatic pressing technique. The ceramic cylinders were cut from larger samples and machined (ground or spark eroded) to final shape. Data are presented in Table 2 for the projectile materials and in Table 3 for the target materials.

The confinement was provided by a tube with a front and a rear plug. The plugs were locked to the tube by threads and by two locking rings welded to the ends of the tube. They were made of tempered steel (SIS 2541-3, comparable to AISI/SAE 4340, flow stress 750 MPa). The tube and the rings were made of marageing steel (Mar 350, flow stress 2.6 GPa).

The inner diameter of the tube was slightly smaller (0.07 mm) than the diameter of the ceramic cylinder. The tube was heated to about 475°C before the ceramic cylinder was inserted (shrink fit). The front and rear plugs were mounted after cooling and tightened with a torque of 26 Nm. Finally, the two locking rings were EB-welded to the tube.

Two 150 kV X-ray flashes were used to determine the impact velocity v_p. The first was triggered at impact and the second after the interaction of target and projectile had ended. The velocity obtained with the aid of the resulting doubly exposed picture slightly underestimates

Table 3
Target material data

Target material	Poisson's ratio ν	Density ρ_p (kg/m^3)	Hardness HV (GPa)	Yield strength σ_y (GPa)
SiC 1	0.17	3220	21.6	10.4
SiC 2	0.16	3180	20.3	9.8
TiB_2	0.19	4400	20.6	9.9
B_4C	0.17	2500	33.0	15.8
Syndie	0.07	4100	71.0	34.1

(by approximately 10–20 m/s) the impact velocity because of the retardation of the target by the projectile.

Four 450 kV X-ray flashes, positioned at the same radial distance from the centre line but separated by 30°, were used to record the penetration process. The penetration depth P in the ceramic was determined from the X-ray pictures using image-processing techniques. The inaccuracy in the measurement of penetration depth was of the order of $\pm$ 0.20 mm. The instants of time t of X-ray flashes were measured within 0.1 μs. The penetration depth data were used to calculate the average penetration velocity u over the observed time interval by means of linear regression.

The X-ray flashes were triggered by means of a pulse caused by the short circuit of two insulated copper wires (diameter 0.07 mm) glued onto the front end of the stationary projectile.

The hardness of the ceramic materials was measured at different loads in the range 50 mN–150 N with the use of a diamond indenter. The machines used were a Nano Indenter IIs (Berkovich diamond tip), a Microhardness tester, MXT-$\alpha \times 1$ Matsuzawa and a JJ Lloyd Instrument hydraulic testing machine (M30K). The average hardness over the upper part of the tested load interval, where the hardness was nearly constant, was used to calculate the yield strength σ_y of the ceramic materials [16,17].

4. Results

Results obtained from the tests are shown in Figs. 4–7. Fig. 4 shows two representative flash X-ray picture sequences of the projectile and the target. Fig. 4(a) illustrates a case of interface defeat, where no significant penetration occurs, and Fig. 4(b) one of normal penetration. Fig. 5 shows a more detailed picture of interface defeat (molybdenum projectile and silicon carbide (SiC-1) target at 21.6 μs after impact).

Fig. 6 shows the penetration for different combinations of metallic projectiles and ceramic targets versus time after impact. The corresponding penetration velocities versus impact velocity are presented in Table 4 and Fig. 7. Observed intervals for the transition impact velocities are presented in Table 5. The lower limit is the highest impact velocity employed without significant penetration, and the upper limit is the lowest impact velocity employed with significant penetration. These intervals are indicated with grey zones in Fig. 7. The continuous u vs. v_p curves in the figure are based on Tate's model [18] and serve as references for the experimental data points.

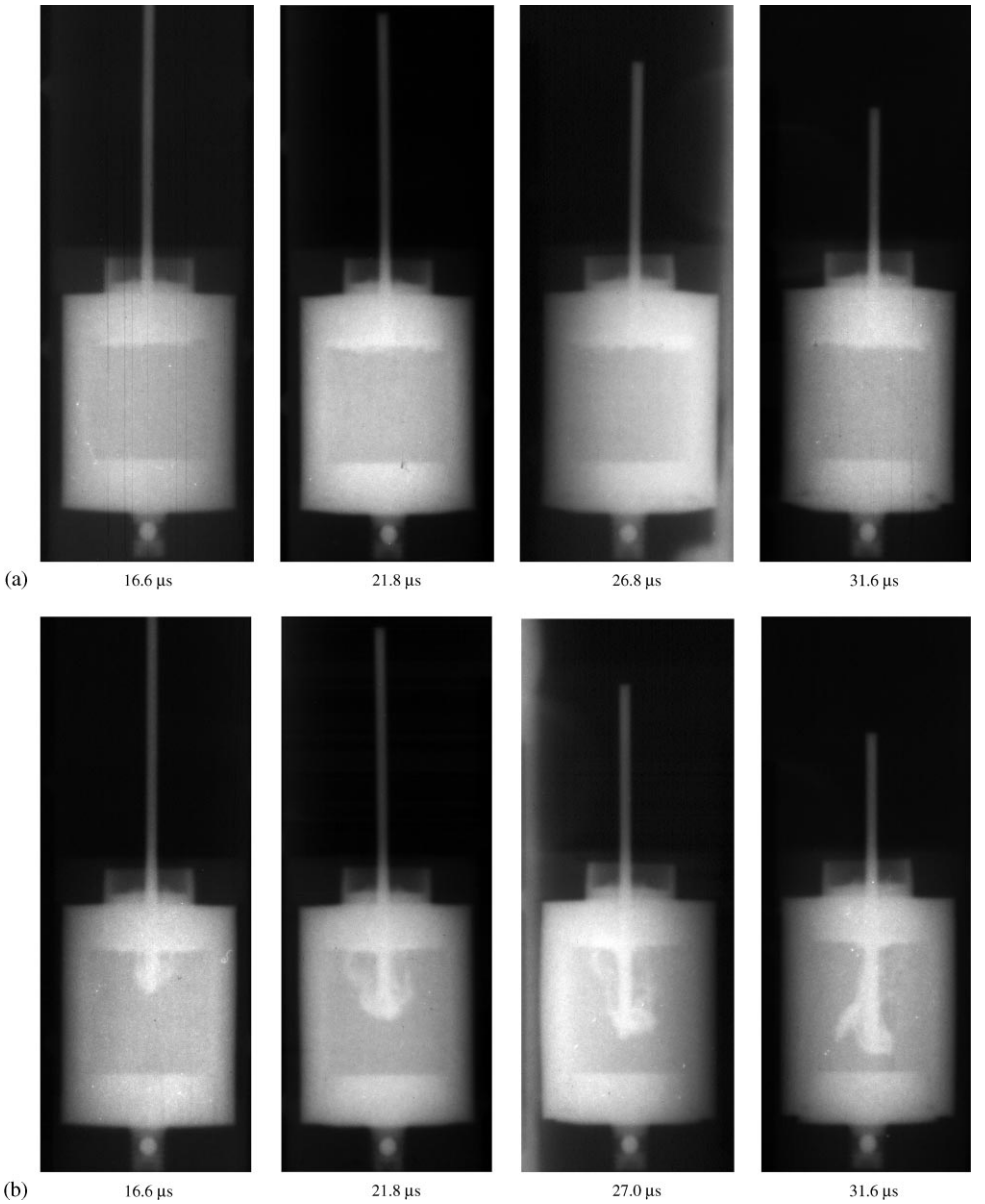

Fig. 4. X-ray pictures of tungsten projectile and silicon carbide (SiC-2) target at four different times after impact. (a) Test 241. Impact velocity $v_p = 1615$ m/s, slightly below transition. (b) Test 242. Impact velocity $v_p = 1805$ m/s, slightly above transition.

Fig. 6. Penetration P versus time t for tests indicated by impact velocity in m/s and test number in parenthesis. (a) Tungsten projectile and silicon carbide (SiC-1, SiC-2) target. (b) Tungsten projectile and titanium diboride target. (c) Tungsten projectile and Syndie target. (d) Molybdenum projectile and silicon carbide (SiC-1) target.

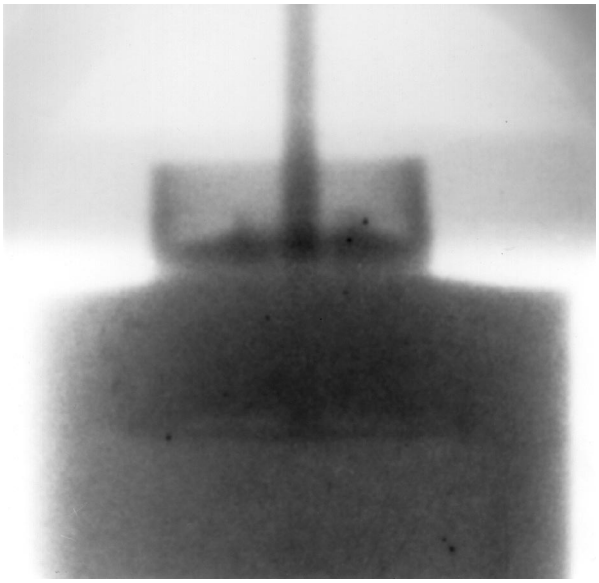

Fig. 5. X-ray picture of molybdenum projectile and silicon carbide (SiC-1) target 21.6 μs after impact. Test 240. Impact velocity $v_p = 2090$ m/s, slightly below transition.

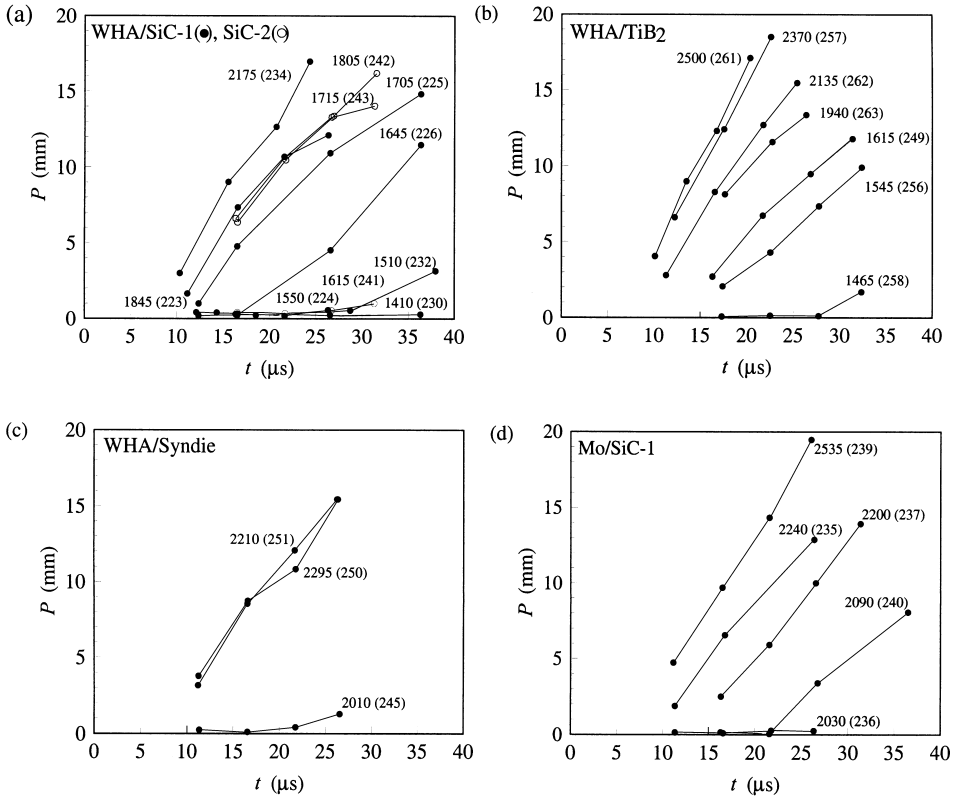

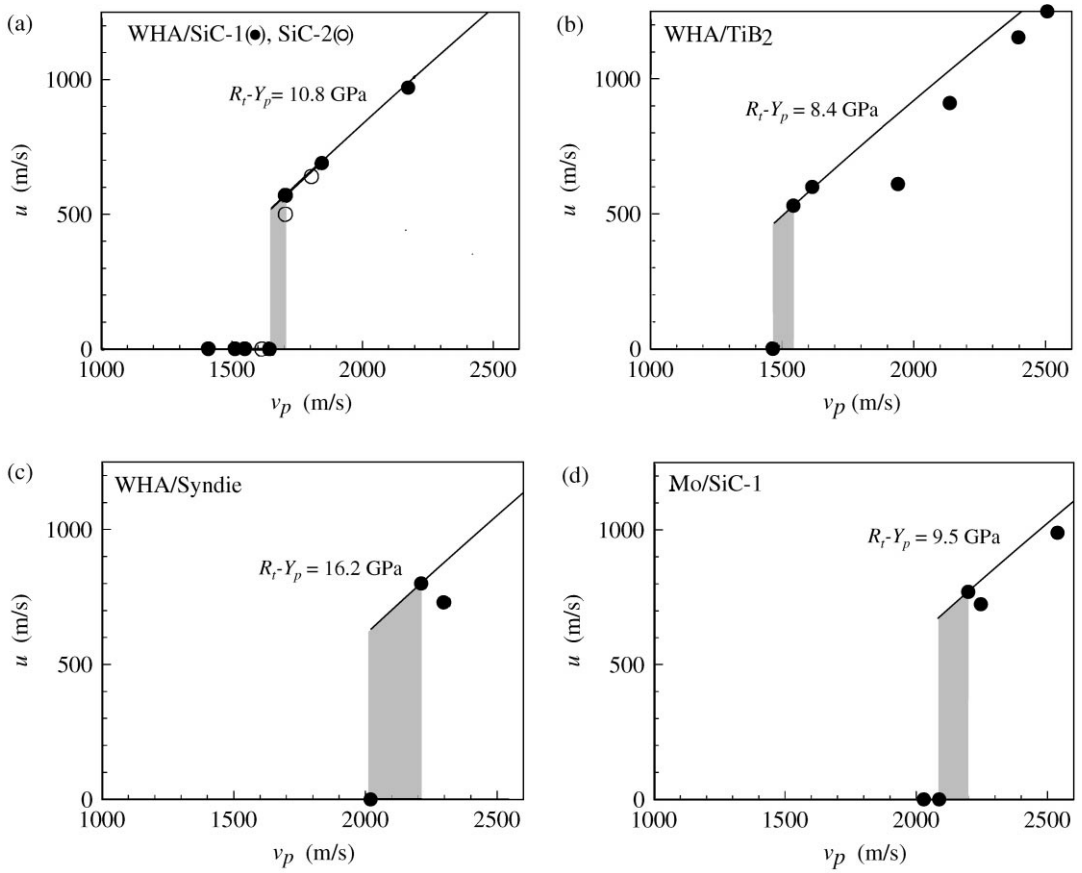

Fig. 7. Penetration velocity u versus impact velocity v_p. (a) Tungsten projectile and silicon carbide (SiC-1, SiC-2) target. (b) Tungsten projectile and titanium diboride target. (c) Tungsten projectile and Syndie target. (d) Molybdenum projectile and silicon carbide (SiC-1) target. Shaded areas indicate region within which transition occurs. The curve in the penetration and transition regions refers to Tate's model.

The differences $R_t - Y_p$ between target and projectile strengths above the transition velocity have been determined in such a way that the Tate curves pass through the points (indicated with a filled circle) representing the lowest impact velocities employed which resulted in significant penetration velocities.

Figs. 8 and 9 show the intervals for the transition velocities obtained from the experimental tests (indicated by vertical bars) and the lower and upper bounds for these velocities (separated by shaded areas) determined from Eqs. (1)–(3) and the inequality (6). The transition velocity data for tungsten projectile and boron carbide target (B_4C) in Table 3 and Fig. 8 have been reported earlier [5].

Table 4
Impact and penetration velocity data for different combinations of projectile and target

Test no.	Projectile/target	Impact velocity v_p (m/s)	Penetration velocity u (m/s)
223	WHA/SiC-1	1845	690
224	WHA/SiC-1	1550	0
225	WHA/SiC-1	1705	570
226	WHA/SiC-1	1645	0 ($t < 20$ μs)
230	WHA/SiC-1	1410	0
232	WHA/SiC-1	1510	0 ($t < 28$ μs)
234	WHA/SiC-1	2175	970
241	WHA/SiC-2	1615	0
242	WHA/SiC-2	1805	640
243	WHA/SiC-2	1715	500
235	Mo/SiC-1	2240	720
236	Mo/SiC-1	2030	0
237	Mo/SiC-1	2200	770
239	Mo/SiC-1	2535	980
240	Mo/SiC-1	2090	0 ($t < 22$ μs)
249	WHA/TiB_2	1615	600
256	WHA/TiB_2	1545	530
257	WHA/TiB_2	2370	1170
258	WHA/TiB_2	1465	0 ($t < 27$ μs)
261	WHA/TiB_2	2500	1250
262	WHA/TiB_2	2135	910
263	WHA/TiB_2	1940	610
245	WHA/Syndie	2010	0 ($t < 22$ μs)
250	WHA/Syndie	2295	730
251	WHA/Syndie	2210	800

Table 5
Transition impact velocities for different combinations of projectile and target

Projectile/target	Transition velocity interval (m/s)
WHA/SiC-1	1645–1705
WHA/SiC-2	1615–1715
Mo/SiC-1	2090–2200
WHA/TiB_2	1465–1545
WHA/Syndie	2010–2210
WHA/B_4C [5]	1430–1480

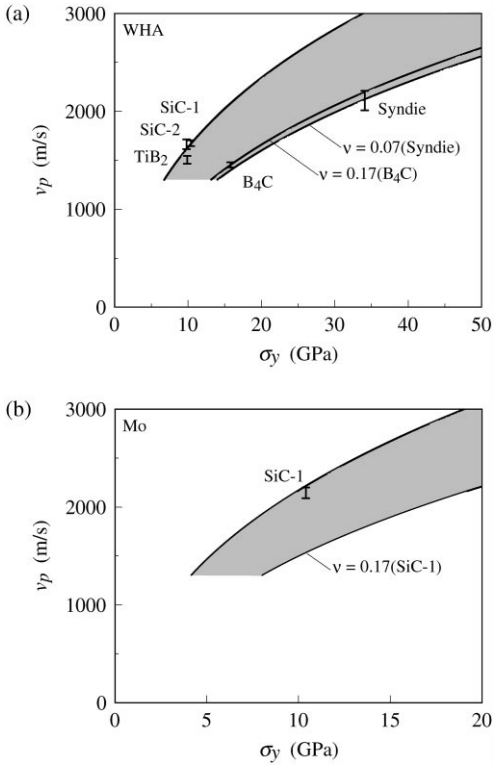

Fig. 8. Transition impact velocity v_p versus target yield strength σ_y for (a) tungsten projectile and (b) molybdenum projectile. The shaded areas correspond to the interval between the estimated lower and upper bounds for the transition impact velocity. The heights of the bars correspond to the intervals of Table 3.

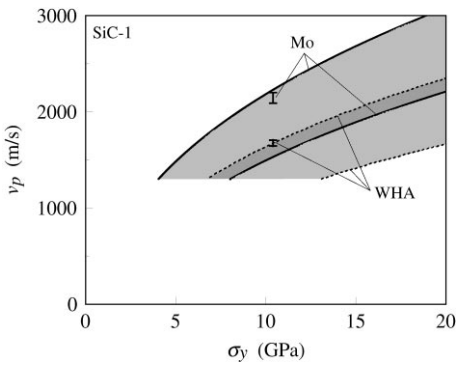

Fig. 9. Transition impact velocity v_p versus target yield strength σ_y for tungsten and molybdenum projectiles and silicon carbide (SiC-1) target. The shaded areas correspond to the interval between the estimated lower and upper bounds for the transition impact velocity. The heights of the bars correspond to the intervals of Table 3.

5. Discussion

A model has been established which makes it possible to estimate the surface load generated by a projectile defeated on the surface of a ceramic target. The projectile was treated as a stationary jet with a certain compressibility (parameter α) and strength (parameter β), and the impact surface was considered to be flat, rigid and friction-free. Thus, the loading was considered to be quasi-static, which is not true initially when the projectile hits the target. In order to establish a similar nearly quasi-static loading experimentally, without damaging the ceramic, some kind of attenuating device has to be used. In this study, such a device was provided by the front plug, which had such thickness that it considerably reduced the initial load on the surface of the ceramic. Yet, a nearly quasi-static loading is very difficult to achieve in practice.

Even under conditions of interface defeat, a certain deformation of the surface of the ceramic target can be expected to occur due to the high surface load. This deformation has some effect on the load distribution on the target, but this effect is not believed to be significant. Another effect of the surface deflection is the generation of radial tensile stresses at the surface of the ceramic. These tensile stresses were reduced in the experimental tests due to the confining action of the tightly shrink-fit steel tube. The confinement also counteracted the effect of the radial shear load due to friction at the interface of target and projectile.

In the analysis, it has been assumed for the projectile that the effect of yield strength is small relative to that of inertia, which means that the dimensionless parameter β defined in Eq. (2) must be small. Comparison with results from numerical simulations suggests that Eq. (1) can be used with fair accuracy for $\beta < 0.135$.

The influence of the yield strength of the projectile in Eq. (1) can be compared to that in Tate's model [18]. When the effect of compressibility is neglected, i.e., $\alpha \to \infty$, Eq. (1) gives

$$p_0 = q_p(1 + 3.27\beta). \tag{7}$$

When the penetration velocity u is zero, Tate's model gives the corresponding result

$$p_0 = q_p(1 + \beta). \tag{8}$$

In these expressions the first terms, which are the same, represent the contribution from inertia, while the terms proportional to β represent the contributions from yield strength. Thus, the contribution from yield strength obtained here is 3.27 times larger than that in Tate's model.

Two pairs of bounds for surface loads and impact velocities have been estimated, viz., lower ones for incipient plastic yield and upper ones for large-scale plastic yield in the target. For the estimated upper bound (5), a slip-line solution for the indentation of a rigid punch was used. Because of the difference between the nearly rectangular distribution of the punch load and the more bell-shaped distribution of the projectile load, it is believed that the estimated upper bound is relatively low and therefore useful.

From the impact tests, transition velocities were determined for the different combinations of metallic projectiles and ceramic targets by using flash X-ray technique. Fig. 4(a) and (b) show tungsten projectiles impacting silicon carbide (SiC-2) targets at impact velocities slightly below and slightly above the transition impact velocity, respectively. Slightly below the transition impact velocity the projectile material flows radially, along the interface of the ceramic and the perforated front plug, without significantly penetrating the ceramic. Slightly above the transition impact velocity, in contrast, the surface load is high enough to overcome the strength of the ceramic which is therefore penetrated by the projectile. At such slightly over-critical impact velocities, the penetration channel deviates from cylindrical shape in an irregular and asymmetric way which was not observed at higher impact velocities. This indicates that the penetration is intermittent and unstable when the impact velocity is slightly above the transition impact velocity. Similar observations have been made also in some previous studies [5,14]. Fig. 5 shows a molybdenum projectile which flows radially on a silicon carbide (SiC-1) surface. In this case there appears to be a certain space between the radially flowing projectile and the inner surface of the front plug. This indicates that the radial flow, once it has been established, can continue without support from the front plug.

It can be seen in Fig. 6 that the slopes of the penetration-versus-time curves for the tests above the transition impact velocities vary with time. Thus, the penetration velocities evaluated using linear fit give only averages of these variable velocities.

Fig. 7 shows that the transition from interface defeat to penetration is quite distinct, which may indicate the presence of some type of material instability. The best agreement with experimental data was obtained for the tungsten projectile and the two types of silicon carbide target. For the tungsten projectile and the titanium diboride target, it is noted that there is a certain disagreement between theoretical and experimental results.

It is noted that the experimentally determined transition impact velocities in Figs. 8 and 9 generally appear near the estimated bounds. Thus, with a tungsten projectile the transition impact velocities are near the estimated upper bound for silicon carbides and titanium diboride and near the estimated lower bound for boron carbide and Syndie. Also, with a molybdenum projectile the transition impact velocity is near the estimated upper bound for silicon carbide (SiC-1).

The indentation method used for determination of the yield strength of ceramic materials appears to give reasonable values. Thus, e.g., the yield strength obtained for silicon carbide (SiC-1) is 10.4 GPa compared with the value 12.5 GPa determined from plate impact tests [19]. Furthermore, the transition velocity ranges determined from the impact tests, inequafllity (6) and Eqs. (1)–(3) lead to similar yield strengths around 10.2 GPa. As the strain rates in the ceramic targets are moderate under conditions of interface defeat, except while the initial transients are present, the use of static yield strengths in the estimation of transition impact velocities is believed to be appropriate.

Acknowledgements

This investigation was financed by the Swedish Armed Forces. Parts of the work on silicon carbide was carried out in co-operation with DERA Chertsey. We thank De Beers for supplying the Syndie material.

Appendix A. Normal surface load per unit area on the axis of symmetry

The rotationally symmetric impact between a long cylindrical projectile and a flat, rigid and friction-free surface is shown in Fig. 1. At large distance from the interface, the stresses in the projectile vanish and the projectile material moves with the axial impact velocity v_p. In terms of cylindrical co-ordinates r and z (no dependence on φ), and under steady-state conditions, the equation of motion in the axial direction is

$$\frac{\partial \sigma_{zz}}{\partial z} + \frac{1}{r}\frac{\partial}{\partial r}(r\sigma_{rz}) = \rho\left(v_r \frac{\partial v_z}{\partial r} + v_z \frac{\partial v_z}{\partial z}\right), \tag{A.1}$$

where σ, v and ρ denote stress, velocity and density, respectively. On the axis of symmetry $r = 0$, the radial velocity v_r is zero, and hence we obtain

$$\frac{\partial \sigma_{zz}}{\partial z}(0, z) = \left[\rho \frac{\partial}{\partial z}\left(\frac{v_z^2}{2}\right) - \frac{1}{r}\frac{\partial}{\partial r}(r\sigma_{rz})\right]_{r=0}. \tag{A.2}$$

In what follows, all relations are to be evaluated on the axis of symmetry, and therefore indications that $r = 0$, such as in relation (A.2), will be left out. Integrating from $z = 0$ to ∞, then, and using the boundary conditions, we obtain

$$-\sigma_{zz}(0) = \rho_p \frac{v_p^2}{2} - \int_0^\infty \frac{\partial \rho}{\partial z} \frac{v_z^2}{2}\, dz - \int_0^\infty \frac{1}{r} \frac{\partial}{\partial r} (r\sigma_{rz})\, dz, \tag{A.3}$$

where partial integration has been carried out on the first term of the right-hand side. This relation can be expressed as

$$-\sigma_{zz}(0) = q_p(1 + \phi + \psi), \tag{A.4}$$

where

$$q_p = \frac{1}{2}\rho_p v_p^2, \quad \phi = -\frac{1}{q_p}\int_0^\infty \frac{\partial \rho}{\partial z} \frac{v_z^2}{2}\, dz, \quad \psi = -\frac{1}{q_p}\int_0^\infty \frac{1}{r} \frac{\partial}{\partial r} (r\sigma_{rz})\, dz. \tag{A.5}$$

The quantity ϕ, which represents elastic effects, is evaluated as follows. If the shear strength of the projectile material is neglected here in comparison with the mean stress σ_m, there is a hydrostatic state of stress $\sigma_{rr} = \sigma_{\varphi\varphi} = \sigma_{zz} = \sigma_m$ and $\sigma_{r\varphi} = \sigma_{\varphi z} = \sigma_{zr} = 0$. Hence, Eq. (A.2) gives

$$\frac{\partial \sigma_m}{\partial z} = \rho_p \frac{\partial}{\partial z}\left(\frac{v_z^2}{2}\right), \tag{A.6}$$

where it has been assumed that $\rho = \rho_p$. Integrating this relation from $z' = z$ to ∞, and using the boundary conditions, we obtain

$$-\sigma_m = \tfrac{1}{2}\rho_p v_p^2 - \tfrac{1}{2}\rho_p v_z^2. \tag{A.7}$$

The mean stress σ_m is also related to the density ρ through the relation

$$\sigma_m = -K_p\left(\frac{\rho}{\rho_p} - 1\right), \tag{A.8}$$

where K_p is the bulk modulus. With the aid of relations (A.7) and (A.8) we can now express the derivative $\partial\rho/\partial z$ in the second of relations (A.5) as

$$\frac{\partial \rho}{\partial z} = -\frac{\rho_p}{K_p}\frac{\partial \sigma_m}{\partial z} = -\frac{\rho_p^2}{K_p}\frac{\partial}{\partial z}\left(\frac{v_z^2}{2}\right). \tag{A.9}$$

Substituting into the second of relations (A.5), we obtain

$$\phi = \frac{1}{q_p}\int_0^\infty \frac{\rho_p^2}{K_p}\frac{v_z^2}{2}\frac{\partial}{\partial z}\left(\frac{v_z^2}{2}\right) dz = \frac{1}{2}\frac{\rho_p^2}{q_p K_p}\left(\frac{v_p^2}{2}\right)^2. \tag{A.10}$$

From relation (A.7) we obtain $\sigma_m(0) = -(1/2)\rho_p v_p^2$. Substituting this relation and $q_p = (1/2)\rho_p v_p^2$ into relation (A.10) we get

$$\phi = -\frac{1}{2K_p}\sigma_m(0). \tag{A.11}$$

On the axis of symmetry at the projectile-target interface $z = 0$, the shear stresses $\sigma_{r\varphi}, \sigma_{\varphi z}$ and σ_{zr} are zero. Hence, the principal stresses are $\sigma_{rr} = \sigma_{\varphi\varphi}$ and σ_{zz}, and von Mises yield criterion gives

$$\sigma_{\mathrm{m}}(0) = \sigma_{zz}(0) + \frac{2}{3}\sigma_{\mathrm{yp}}. \tag{A.12}$$

Substitution into (A.11) gives

$$\phi = -\frac{1}{2\alpha}\left(\frac{\sigma_{zz}(0)}{q_{\mathrm{p}}} + \frac{2}{3}\beta\right), \tag{A.13}$$

where

$$\alpha = \frac{K_{\mathrm{p}}}{q_{\mathrm{p}}}, \quad \beta = \frac{\sigma_{\mathrm{yp}}}{q_{\mathrm{p}}}. \tag{A.14}$$

The quantity ψ, which represents plastic effects, is determined as follows. It is assumed that beyond a distance b from the projectile-target interface, the projectile is in a state of uniaxial stress with $\sigma_{rz} = 0$. Then, the integration interval in the third of relations (A.5) is limited to $z \in [0, b]$. In this interval, the projectile material is assumed to flow as a perfectly-plastic solid obeying von Mises yield criterion and the associated flow rule

$$\sigma_{rz} = \frac{\sqrt{6}}{3}\sigma_{\mathrm{yp}}\frac{d_{rz}}{|\,\mathbf{d}\,|}, \tag{A.15}$$

where $\mathbf{d}$ is the rate of deformation tensor with rz-component and norm

$$d_{rz} = \frac{1}{2}\left(\frac{\partial v_r}{\partial z} + \frac{\partial v_z}{\partial r}\right), \quad |\,\mathbf{d}\,| = \sqrt{d_{ij}d_{ij}} = \sqrt{\left(\frac{\partial v_r}{\partial r}\right)^2 + \left(\frac{\partial v_z}{\partial z}\right)^2 + \left(\frac{v_r}{r}\right)^2 + 2\left(\frac{\partial v_r}{\partial z} + \frac{\partial v_z}{\partial r}\right)^2}, \tag{A.16}$$

respectively. Substituting relation (A.15) into the third of relations (A.5), we obtain

$$\psi = -\frac{\sqrt{6}}{3}\beta\int_0^b \frac{1}{r}\frac{\partial}{\partial r}\left(r\frac{d_{rz}}{|\,\mathbf{d}\,|}\right)\mathrm{d}z. \tag{A.17}$$

This expression is evaluated using a rate of deformation tensor $\mathbf{d}$ for a potential velocity field (incompressible and non-viscous). The boundary conditions are taken to be such, that (i) the stress field in the projectile is continuous at $z = b$ with $b = 3a$ [6] and (ii) the axial velocity $v_z = 0$ at the projectile-target interface $z = 0$. The continuity of the stress field at $z = b$ implies that the rate of deformation field must have a jump. This jump is assumed here to be proportional to β for $\beta \ll 1$. With these assumptions ψ is obtained from relation (A.17) as

$$\psi \approx 3.27\,\beta, \tag{A.18}$$

for $\beta \ll 1$.

Substituting Eqs. (A.13) and (A.18) into Eq. (A.4), we finally obtain the maximum normal stress at the projectile–target interface

$$-\sigma_{zz}(0) = p_0 \approx q_{\mathrm{p}}\left(1 + \frac{1}{2\alpha} + 3.27\beta\right) \tag{A.19}$$

for $\alpha \gg 1$ and $\beta \ll 1$.

References

[1] Shockey DA, Marchand AH, Skaggs SR, Cort GE, Burkett MW, Parker R. Failure phenomenology of confined ceramic targets and impacting rods. Int J Impact Engng 1990;9:263–75.
[2] Hauver GE, Netherwood PH, Benck RF, Kecskes, LJ. Ballistic performance of ceramic targets. Army Symposium on Solid Mechanics, USA, 1993.
[3] Hauver GE, Netherwood PH, Benck RF, Kecskes LJ. Enhanced ballistic performance of ceramic targets. Proceedings of the 19th Army Science Conference, USA, 1994.
[4] Rapacki EJ, Hauver GE, Netherwood PH, Benck RF. Ceramics for armours — a material system perspective. Proceedings of the 7th Annual TARDEC Ground Vehicle Survivability Symposium, USA, 1996.
[5] Lundberg P, Holmberg L, Janzon B. An experimental study of long rod penetration into boron carbide at ordnance and hyper velocities. Proceedings of the 17th International Symposium on Ballistics, South Africa, Vol. 3, 1998. p. 251–65.
[6] Reich F. Omlenkung eines freien Flussigkeitsstrahles an einer zur Strömungsrichtung senkrecht stehenden ebenen Platte. Diss Hannover: 1926, (oder VDI-Forsch.-Heft 290).
[7] Fung YC. Foundations of solid mechanics. Englewood Cliffs, NJ: Prentice-Hall, 1965.
[8] Hencky H, Angew Z. Mat Mech 1923;3:241.
[9] Haar A, von Kármán Th. Nacher Ges Wiss Göttingen, Math Phys Kl, 1909; p. 204.
[10] Shield RT. On the plastic flow of metals under conditions of axial symmetry. Proc R Soc A 1955;233:67.
[11] Hill R. The mathematical theory of plasticity. Oxford: Clarendon Press, 1998.
[12] Subramanian R, Bless SJ. Penetration of semi-infinite AD995 alumina targets by tungsten long rod penetrators from 1.5 to 3.5 km/s. Int J Impact Engng 1995;17:807–16.
[13] Orphal DL, Franzen RR, Piekutowski AJ, Forrestal MJ. Penetration of confined aluminum nitride targets by tungsten long rods at 1.5 to 4.5 km/s. Int J Impact Engng 1996;18:355–68.
[14] Orphal DL, Franzen RR. Penetration of confined silicon carbide targets by tungsten long rods at impact velocities from 1.5 to 4.6 km/s. Int J Impact Engng 1997;19:1–13.
[15] Orphal DL, Franzen RR, Charters AC, Menna TL, Piekutowski AJ. Penetration of confined boron carbide targets by tungsten long rods at impact velocities from 1.5 to 5.0 km/s. Int J Impact Engng 1997;19:15–29.
[16] Zeng K, Söderlund E, Giannakopoulos AE, Rowcliffe DJ. Controlled indentation: a general approach to determine mechanical properties of brittle materials. Acta Mater 1996;44(3):1127–41.
[17] Zeng K, Rowcliffe D. Analysis of penetration curves produced by sharp indentations on ceramic materials. Philos Mag A 1996;74(5):1107–16.
[18] Tate A. Further results in the theory of long rod penetration. J Mech Phys Solids 1969;17:141–50.
[19] Bourne N, Millett J, Pickup I. Delayed failure in shocked silicon carbide. J Appl Phys 1997;81(9):6019–23.